RSC Advances

ROYAL SOCIETY OF CHEMISTRY

www.rsc.org/advances

Cite this: DOI: 10.1039/c0xx00000x

www.rsc.org/xxxxxx

ARTICLE TYPE

Heteroatom doped porous carbon derived from hair as anode with high performance for lithium ion batteries

Junke Ou,[a] Yongzhi Zhang,[b] Li Chen,[c] Hongyan Yuan*[c] and Dan Xiao*[a,b,c]

Received (in XXX, XXX) Xth XXXXXXXXX 20XX, Accepted Xth XXXXXXXXX 20XX

DOI: 10.1039/b000000x

Heteroatom doped porous carbon (HDPC) are fabricated using human hair as carbon source via acid pretreatment procedure and sequent KOH activation. With the introduction of acid pretreatment, the obtained HDPC possesses a large specific surface area and appropriate heteroatom doping level. As anode material for lithium ion battery, the as-synthesized HDPC delivers a superior specific capacity of 1331 mAh g^{-1} at 0.1 A g^{-1} and shows an impressive rate capability of 470 mAh g^{-1} at 5 A g^{-1}. Even at an ultrahigh current density of 10 A g^{-1}, the reversible capacity is still as high as 205 mAh g^{-1}. The excellent electrochemical performance of HDPC could be ascribed to the high specific surface area, well-formed micro- and mesoporosity and heteroatom doping effects.

.

Introduction

Confronted with increasing crude oil prices and global warming, much effort has been focused on development of power sources for hybrid electric vehicles (HEVs) and renewable energy systems. Rechargeable lithium ion batteries (LIBs) with high energy density and long life cycle have became the most suitable energy storage device for these applications compared to any existing battery systems.[1] It is well known that graphite is the most popular commercial anode material for LIBs due to its low cost and low electrochemical potential with respect to lithium metal.[2,3] However, its limited storage capacity is only 372 mAh g^{-1}(corresponding to the first-stage graphite intercalation compound, LiC_6), and its rate performance cannot meet the demand for LIBs with high energy and high power. Therefore, much attention has been delivered to the exploration of new carbon materials that have fast kinetics of lithium ion insertion/de-insertion.[4,5]

Carbon-based material, especially nanostructured porous carbon material, being a three-dimensional (3D) conductive network, has been demonstrated to be attractive. The reversible lithium insertion–extraction capacity of the porous carbon material is much higher than that of the commercially available graphite. Moreover, the nanopores can enhance diffusion kinetics by shortening the distance of lithium ion diffusion and facilitating the transmission of electrons, improving the rate performance.[6,7] Meanwhile, its cycling performance could be greatly enhanced owing to the lack of a large volume change of the carbon host, resulting from the existence of interconnected pores, which could act as the buffer layers to reduce the volume change during the Li insertion and extraction.[8] Porous carbons are usually prepared through templating methods using mesoporous silica, zeolites and close-packed poly (methyl methacrylate) spheres as hard templates, and amphiphilic copolymer surfactants as soft templates.[9-12] For example, Hu et al. prepared hierarchical porous carbon monoliths with an initial reversible capacity of 900 mAh g^{-1} at C/5 and good rate performance.[7] Rod-shaped ordered mesoporous carbons (OMCs) with different lengths prepared by size-tunable SBA-15 silica deliver a reversible capacity as high as 1012 mAh g^{-1}.[9] However, such templating approaches are tedious, time- and energy-consuming, which is hard to be scaled up for mass production.

Recently, as a renewable source, biomass as a carbonaceous precursor has become more and more attractive for its abundance, low cost, easy accessibility and environmental friendliness compared with other carbonaceous precursors.[13,14] Utilizing sustainable biomass for the energy applications has received much attention in the scarcity of fossil energy. Hence, porous carbons derived from biomass as anode for LIBs have been explored with sources as diverse as cotton wool, coconut, starch, coffee shells, banana fibers, husk rice, rice straw, algae, cherry stones, pinecone hull and wheat straw.[15-26] Apart from above biomass materials, organically rich human wastes for LIBs anodes with high electrochemical performances have rarely been reported.

Human hair, a filamentous biomaterial that grows from follicles of dermis in the major part of lifetime, is one of the abundantly available organic wastes. It contains about 51% carbon, 17% nitrogen, 21% oxygen, 6% hydrogen, 5% sulfur, and trace amounts of iron, magnesium, arsenic, chromium and

various minerals.[27-29] However, most human hair is still dumped as a waste. Few studies concerning the preparation of carbon materials from human hair are reported. Recently, human hair was applied as a precursor material to prepare a carbon material for supercapacitors and the oxygen reduction reaction (ORR).[30-31] Biomass (such as rice straw and rice husk) activated by KOH had been reported as carbon anodes and showed high reversible capacities.[20-21] However, their electrochemical performances are undesirable.

Another approach to improve the electrochemical performance for the carbon-based anodes is to incorporate non-carbon elements (N, B, P, and S) in the carbon structure. The presence of heteroatom at the carbon surface can enhance the reactivity and provide pseudocapacitance and extra Li-ion storage sites.[32-36] For instance, LIBs anode applying N-doped mesoporous carbon derived from egg white exhibited ultra-high capacity of 1780 mAh g^{-1} at the current density of 100 mA g^{-1}, thus emphasizing the untapped potential of biomass being used to prepare carbon materials for energy storage.[32]

In this paper, we report a simple and effective strategy in preparing heteroatom doped porous carbon material (HDPC) from human hair. Human hair is rich in nitrogen and sulfur, which is an ideal precursor for the preparation of heteroatom doped carbon materials. N and S dual-doped porous carbon materials along with high specific surface area were produced through acid pretreatment and KOH activation. Benefiting from the unique porous structure and appropriate N and S doping, the HDPC exhibits significantly high reversible capacity as the anode material for LIBs, showing a capacity of as high as 1325 mAh g^{-1} at the current density of 0.1 A g^{-1} even after 200 cycles. In addition, creating high-performance carbon material from the discarded hair provides a strategy for its disposal issue and contributes to the environmental improvement.

Experimental section

Sample preparation

The human hair obtained from barbershops was cleaned by deionized water, ethanol and dried. The prepared hair was cut into small pieces(～5 mm long) and refluxed with 1.0 M HCl solution at 120 □ in an oil bath for 2 h. To remove the residual acid, the obtained product was washed with deionized water till the filtrate became neutral. Then the dried sample was impregnated in KOH solution (the amount of KOH to hair ratio in terms of weight was 3:1) for 24 h and dried in an oven at 120 ℃. The obtained substance was carbonized at 700 ℃ for 2 h with a heating rate of 5 ℃ min^{-1} in a horizontal tube furnace under Ar atmosphere. Finally, the black solid was thoroughly washed with deionized water to ensure it was neutral and dried in an oven at 80 ℃ for 12 h. The preparation process of heteroatom doped porous carbon (HDPC) derived from human hair is displayed in Fig. S1 (ESI†). For comparison, the human hair not treated by HCl and KOH (NH-C) and human hair only activated by KOH (AH-C) were also prepared at 700 ℃ for 2 h under Ar flow.

Characterization of the materials

The obtained samples were subjected to various characterization techniques. X-ray powder diffraction (XRD) patterns of the products were recorded on a TD-3500 X-ray powder diffractometer (Tongda, China). Raman spectra were recorded with a confocal LabRAM HR800 spectrometer, HORIBA Jobin Yvon, France. XPS were recorded using a Kratos XSAM 800 spectrometer (Manchester,UK). Energy dispersive spectroscopy (EDS) fluorescence measurements were taken with a spectrometer attached to a Hitachi S4800 field emission scanning electron microscopy (FESEM). The transmission electron microscopy (TEM) images were performed using a FEI Tecnai G2 20 TEM (Hillsboro, OR, USA). Digital photographs were taken with a NIKON D3100 DSLR Camera. Nitrogen adsorption and desorption isotherms were determined with a micrometeretics tristar 3020 automatic analyzer (USA). The samples were degassed at 300 ℃ for 6 h before absorption measurements. Specific surface areas were estimated according to the BET model, and pore size distributions were calculated by using the NLDFT method.

Electrochemical measurements

Electrochemical performance was conducted using coin-type (CR 2032) cells with metallic lithium foil as the counter electrode. The working electrode was prepared by depositing the mixed slurry of active material, acetylene black and poly (vinyl difluoride) (PVDF) with a weight ratio of 8: 1: 1 onto Cu foil, and then drying at 100 ℃ under vacuum. Each working electrode contained about 2 mg of active materials and had a geometric surface area of circular 1.53 cm^2. The electrolyte consisted of a solution of 1M $LiPF_6$ in ethylene carbonate (EC)/dimethyl carbonate (DMC) (1:1, in wt%).The charge/discharge tests were performed between 0.0-3.0 V (vs. Li^+/Li) on a Newware CT-3008W battery cycler (Guangdong, China). Cyclic voltammetry (CV) measurements were performed at a scanning rate of 0.1 mV s^{-1} on an Autolab PGSTAT 302 electrochemical workstation in the voltage range of 0.0-3.0 V. Electrochemical impedance spectroscopy (EIS) was carried out in the frequency range 0.01-100 kHz at a charged stage with an applied amplitude of 5 mV.

Results and Discussion

KOH immersing leads to a homogeneous mixture of them, and KOH oxidatively reacts with carbon at high temperature to generate H_2, CO_2 and CO gas and thus produce the pores.[37] The activation mechanism of KOH is as below:

$$6KOH + 2C \longrightarrow 2K + 3H_2 + 2K_2CO_3 \quad (1)$$

$$K_2CO_3 \longrightarrow K_2O + CO_2 \quad (2)$$

$$CO_2 + C \longrightarrow 2CO \quad (3)$$

$$K_2CO_3 + 2C \longrightarrow 2K + 3CO \quad (4)$$

$$K_2O + C \longrightarrow 2K + CO \quad (5)$$

X-ray diffraction (XRD) patterns of the three samples were displayed in Fig. 1a. There are two broad peaked around 23.6° and 43.6°, corresponding to the (002) and (100) reflections of carbon, respectively, which indicates that the sample is predominantly made up of single-layer carbon sheets that are not stacked in a parallel fashion. Hence, there must be small pores or voids between the carbon sheets.[11] Furthermore, no sharp peaks are observed in the XRD patterns of the AH-C and HDPC,

demonstrating their amorphous structure, which is favorable for lithium ion intercalation and deintercalation.[38] Raman spectra which have been widely used to characterize carbon materials are sensitive to the slight structural changes. As presented in Fig. 1b, a prominent D band is located at 1338 cm^{-1}, which is ascribed to edges and disorder carbon in the carbon structures. A typical G band at 1585 cm^{-1} is associated with ordered sp^2 bonded carbon.[39] Generally, the intensity ratio of the I_D/I_G stands for disorder degree and the average size of the sp^2 domains.[38-40] The I_D/I_G ratio of the HDPC is determined to be 1.01, significantly higher than that of AH-C (I_D/I_G=0.94) and the NH-C (I_D/I_G=0.86). This result suggests that HDPC possessed a higher degree of disorder, more edges, and more other defects (sp^3 bonded carbon, dangling bonds, vacancies, and topological defects), which is beneficial for the increase of reversible capacity of anode and the enhancement in Li storage ability.[8,38]

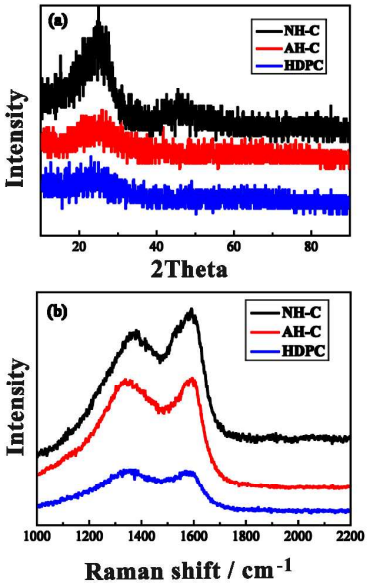

Fig. 1 (a) XRD patterns and (b) Raman spectra of the NH-C, AH-C and HDPC.

Human hair was employed as the raw material to fabricate HDPC not only because it is abundant, widespread and low-cost, but also it possessed large amounts of protein, notably the keratin, which mainly has lots of cysteine, a sulfur-containing amino acid. However, trace metallic elements (such as iron, magnesium, arsenic and chromium) are existed in the hair.[27-29] These elements may occupy some active sites and affect the Li storage. Therefore, acid pretreatment was introduced to remove these metallic elements. The micrograph of human hair was characterized by scanning electron microscopy (SEM)(Fig. 2a). A scaled lamellar structure was clearly observed. After the acid pretreatment, more dense scaled structures were found on the surface of hair (Fig. S2, ESI†), which might be due to the elimination of some metallic elements and the destruction of cuticle. Meanwhile, the results of Energy dispersive spectroscopy (EDS) and total XPS spectrum also confirm that metallic elements could be removed by acid pretreatment (Fig. S3 and Table S1 ESI†). After carbonization of the hair without any treatments (Fig. 2b), some carbon fragments were obtained, which may be owing to the weak interaction between the overlapping scales, and can be easily broken apart. Compared to NH-C, the AH-C presented a loose structure (Fig. 2c). Fig. 2d shows that the HDPC has a more dispersed morphology than that of AH-C. A large amount of nanoscale pores formed a three-dimensional (3D) connected porous structure. The transmission electron microscopy (TEM) and HRTEM images in Fig. 2e-f reveal that large quantities of micropores and mesopores are distributed within HDPC. These micro/mesopores and interconnections of the carbon materials would offer the chemistry and structure to store the lithium ions, and the pore-transport system would ensure the accessibility of those sites by lithium ions.[7,41] Therefore, these porous carbon materials derived from human hair would be expected to be promising electrode materials for LIBs.

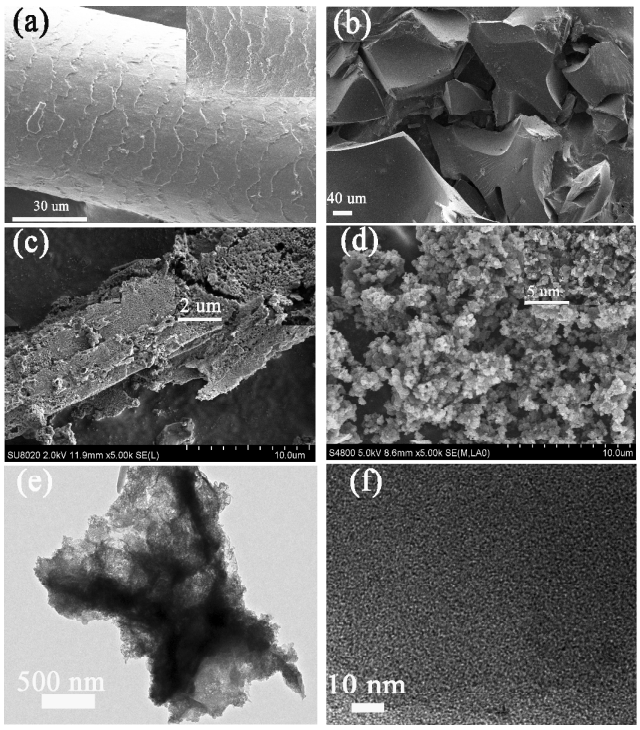

Fig. 2 Scanning electron microscopy (SEM) image of the surface topography of (a) human hair; SEM image of (b) NH-C, (c) AH-C and (d) HDPC; TEM image (e) and HRTEM image (f) of HDPC. (a), (c) and (d) are the partial enlargements of the relevant images

In order to investigate the structure of the carbon material derived from human hair, nitrogen adsorption–desorption isotherms were measured (Fig. 3a). It is clear that NH-C shows a very low amount of adsorbed gas, indicating the non-porous characteristic, while the other two carbons activated by KOH show type I sorption isotherms with a much higher N_2 sorption capacity, indicating the microporous characteristic. The specific Brunauer–Emmett–Teller (BET) surface area of the NH-C is 10 $m^2 g^{-1}$, whereas the specific surface areas of the AH-C and HDPC are increased significantly to 1070 and 1250 $m^2 g^{-1}$. The pore size distributions (PSDs) for the AH-C and HDPC were estimated by non-local density functional theory (NLDFT) and are presented in Fig. 3b. It can be seen that both the AH-C and the HDPC are mainly composed of micropores between 1 and 2 nm. Although

chemical activation generally leads to the micropores in the surface, some mesopores located between 3 and 4 nm were observed in Fig. 3b. The formation of mesopores can be mainly ascribed to the randomly arranged carbon sheets that are not stacked in parallel, as indicated in XRD pattern of Fig. 1.

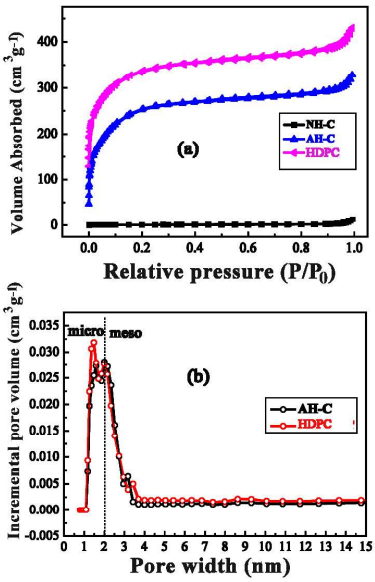

Fig. 3 (a) Nitrogen absorption-desorption isotherms for the NH-C, AH-C and HDPC; (b) pore size distributions (PSDs) for the AH-C and HDPC.

Hair is mainly composed of protein, especially keratin which possesses large amounts of the sulfur-containing amino acid cysteine. Nitrogen (3.5) has a higher electronegativity than carbon (3.0), because its atomic diameter is smaller. In addition, there is a stronger interaction between Li and the N-doped carbon material because of the hybridization of nitrogen lone pair electrons with the π electrons in the carbon. Therefore, the electronegativity and hybridization might be favorable for lithium insertion.[42,43] X-ray photoelectron spectroscopy (XPS, Fig. 4) was employed to further analyze the atom binding states of as-obtained HDPC. As seen in Fig. 4a, the deconvolution of the N 1s spectra yields four peaks: N-6 (398.5±0.2 eV), pyridinic-N; N-5 (399.9 ±0.2 eV), pyrrolic/pyridone-N; N-Q (400.8 ±0.2 eV), quaternary-N; and N-X (402.5 ±0.2 eV), pyridine-N-oxide.[32, 42-43] It should be noted that pyridinic N is more favorable than pyrrolic-N for Li storage and is a significant factor in the enhancement of reversible capacity.[32,43] In addition, the quaternary nitrogen peaked at 402.5 eV could improve the electrical conductivity of carbon materials.[44] As depicted in Fig. 4b, the high resolution S 2p peak can be resolved into three peaks located at 164.2 eV, 168.5 eV and 170.5 eV, respectively. The peak at 164.2 eV can be identified to the species in the state of –C–S–C–, and the other two peaks to the oxidized sulfur in the state of sulfate (–C–SO_4–C–) or sulfonate (–C–SO_3–C–), which may be derived from reaction of surface sulfur with adjacent oxygen molecules.[45,46] The main peak corresponding to –C–S–C– may contribute to an increased reversible capacity.[36] Heteroatom doped carbons contain defects through which lithium ions can perpendicularly diffuse from outside to inside graphite layers, thus providing more Li storage regions.[42] Compared with the chemical post-modification by the treatment of H_2SO_4 and NH_3 for the porous carbon, our work provides a simple method to fabricate heteroatom doped porous carbons. The surface element compositions and porosity parameters of prepared carbons have been summarized in Table 1.

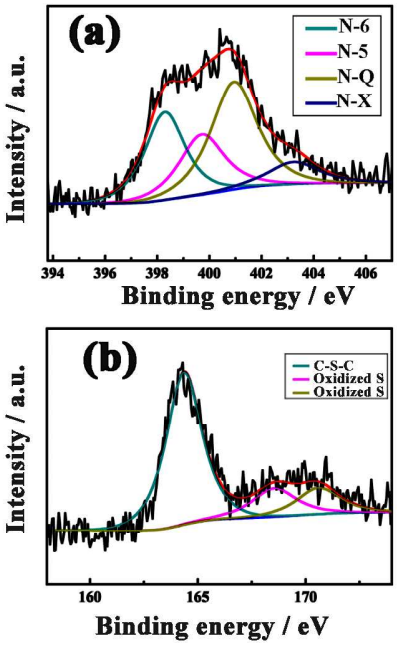

Fig. 4 Deconvoluted N 1s (a) and S 2p (b) of HDPC.

The electrochemical performances of the samples as anode materials for lithium ion batteries were further studied. Fig. 5a shows the first three cyclic voltammograms (CV) curves for HDPC electrode at a scan rate of 0.1 mVs^{-1} in the voltage window of 0.0-3.0 V (vs. Li^+/Li), which exhibits a typical CV behavior of carbon materials in lithium batteries.[32] Fig. 5b-d show the charge–discharge curves of the NH-C, AH-C and HDPC at a current density of 0.1 A g^{-1}, respectively. In the first cycle, the electrode of HDPC delivered a high reversible capacity (1347 mAh g^{-1}) at a current density of 0.1 A g^{-1}(Fig. 5d), much higher than that of other two samples (370 mAh g^{-1} and 960 mAh g^{-1} respectively). After calculation, the initial Coulombic efficiency of the HDPC was 63% at 0.1 A g^{-1}. The large loss in capacity during the first cycle means that a significant part of the lithium is unavailable for reversible reactions. Generally speaking, the large initial capacity fading can be ascribed to the conversion of the carbon electrode from its pristine form to an active lithium storage host; the formation of a solid electrolyte interface (SEI) caused by the catalytic reduction of the electrolyte components on the active electrode surface, and/or irreversible lithium insertion into special positions such as in the vicinity of residual H atoms in the carbon material as it was previously reported in the literature.[7,47] The reversible of HDPC is 1334 mAh g^{-1} in the second cycle, and the Coulombic efficiency of the second cycle increases dramatically to 95%. As the cycling continued to 50th cycle, the reversible capacity of HDPC is maintained at 1331 mA h g^{-1} and the Coulombic efficiency stabilizes to nearly 100%, presumably due to the stabilization of SEI film. However, the other two samples present obviously fading capacities (220 mAh $g^{-1}$and 500 mAh g^{-1} for the electrode of NH-C and AH-C

respectively).

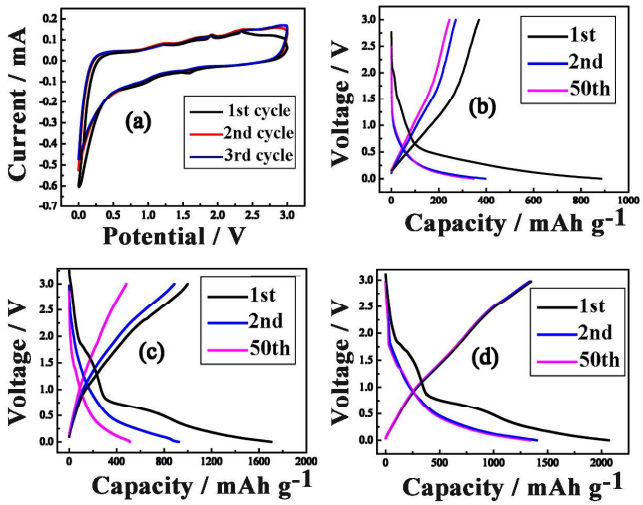

Fig. 5 (a) Cyclic voltammograms of the HDPC at a scan rate of 0.1 mV s^{-1}, the galvanostatic charge and discharge profiles of (b) the NH-C, (c) the AH-C and (d) the HDPC at the current density of 0.1 A g^{-1}.

The reversible capacity of the HDPC is not as high as that of mesoporous nitrogen-rich carbon derived from egg white[32] at a low current density, partly because of its lower N content. However, its rate capability and cycling performance seem not to be affected by this shortcoming. For testing the rate performance of HDPC, the cell was directly charged/discharged at various current densities from 0.1 A g^{-1} to 10 A g^{-1} each for 20 cycles (Fig. 6a). The carbon electrode delivered a reversible capacity of 1331, 1181, 905, 760, 620 mAh g^{-1} at 0.1, 0.2, 0.5, 1, 2 A g^{-1}, respectively. Even at extremely high current densities of 5 and 10 A g^{-1} (13.4 C and 26.8 C, 1 C = 372 mA g^{-1}), the reversible capacities are still as high as 470 and 205 mA h g^{-1}, respectively. High rate capability is an important property of electrode materials for high power LIBs. When the current density decreased back to 0.1 A g^{-1}, the specific capacity recovered to 1329 mAh g^{-1}, which reveals the stable rate performance of HDPC. In addition to its considerable capacity and rate performance, the cycling performance of HDPC was also evaluated during charged/discharged process. As shown in Fig. 6b, an impressive cycling performance was observed, being as high as 1325 mA h g^{-1} and 752 mAh g^{-1} at 0.1 and 1 A g^{-1} respectively even after 200 cycles. The large surface area facilitates good contact of HDPC with electrolyte and further promotes the transportation of lithium ions; the numerous pores may not only act as reservoirs for storage of lithium ions, but also accommodate the local volume change of the carbon anode material, thus effectively alleviating the pulverization issues and leading to a good cycling ability.[8,41] We compared the rate performance and cycling performance of HDPC in this work with major published data on those of some carbon materials derived from biomass as anodes for lithium ion batteries and listed the major characteristics of each report (Table S2, ESI†). Clearly, HDPC present a better electrochemical performance as anode for LIBs. The unique porous structure with high surface area and the favorable defects with nitrogen- and sulfur- doping jointly contribute to the high specific capacity and excellent rate performance.

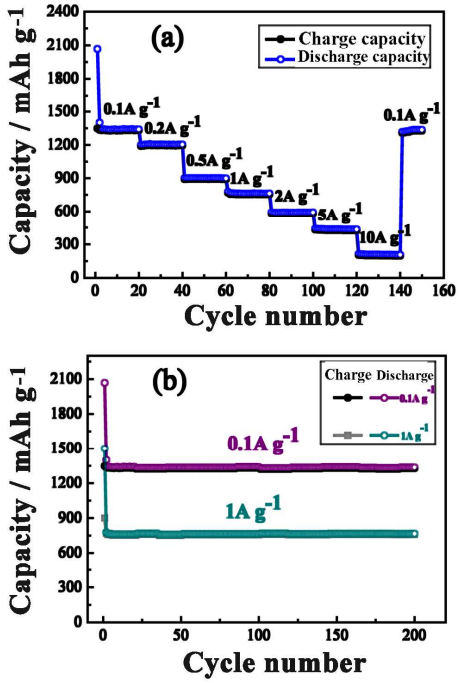

Fig. 6 (a) The rate performance of HDPC over cycling at different current densities; (b) cycling performance of the HDPC at 0.1 A $g^{-1}$and 1.0 A g^{-1}

Table 1 Porosity parameters and elemental composition by X-ray photoelectron spectroscopy (XPS) of the carbon samples.

Sample	Porosity parameters							XPS (atom%)		
	S_{BET} (m^2 g^{-1})	S_{micro} (m^2 g^{-1})	S_{meso} (m^2 g^{-1})	V_{pore} (cm^3g^{-1})	V_{micro} (cm^3 g^{-1})	V_{meso} (cm^3 g^{-1})	D_{aver} (nm)	C	N	S
NH-C	10	8	2	0.005	0.0045	0.0005	27	84.35	4.05	2.08
AH-C	1070	960	110	0.53	0.39	0.14	2.14	83.75	4.11	2.12
HDPC	1250	1132	118	0.66	0.49	0.17	2.05	85.37	4.24	2.23

To further investigate the reason of good electrochemical performance of the as-prepared HDPC. EIS measurements were carried out for the three samples after testing up to 10 cycles of galvanostatic charge/discharge at 0.1 A g^{-1}, and the representative Nyquist plots are presented in Fig. 7. The Nyquist plots for three electrodes consist of a depressed semicircle in the high and middle frequency regions and a straight line in the low frequency region. According to the previous papers, the high-frequency semicircle is attributed to SEI film and/or contact resistance, the semicircle in medium-frequency region is assigned to the charge-transfer impedance on electrode/electrolyte interface, and the inclined line at an approximate 45° angle to the real axis corresponds to the Li diffusion process within carbon electrodes.[48] The impedance of the electrodes was fit using the modified equivalent circuit shown in the inset of Fig. 7. R_e is the total resistance of the electrolyte, electrode and separator, CPE1 and R_f are the surface film capacitance and the resistance for lithium ion migration through the SEI film, respectively. In addition, CPE2 and R_{ct} are the double layer capacitance and charge transfer resistance, respectively; Z_w is the Warburg impedance related to the lithium ion diffusion in the inserted materials; and C1 is related to the insertion capacitance reflecting the occupation of lithium into the inserted sites.[49-50] The fitting values from the proposed equivalent circuit are listed in Table 2. It can be clearly seen that the R_{ct} of HDPC electrode are 18.23 Ω, which are much smaller than that of the other two electrodes, indicating the faster charge and mass transfer in the lithium insertion–extraction process and the facile charge transfer at the electrode/electrolyte interface. Broadly speaking, a high specific area causes more side reactions that thicken the SEI film. However, the R_f of HDPC is 9.35 Ω, lower than that of the NH-C (11.16 Ω) and the AH-C (12.31 Ω), meaning that the lithium ions in the HDPC can pass through the SEI film more easily than that in the NH-C or AH-C. This can be attributed to the slightly increase in N and S contents of the HDPC, which can suppress the electrolyte decomposition and surface side reactions of the electrodes with the electrolyte, reduce the formation of the SEI film.[51-52] Furthermore, the micro-/meso-pores supply facile storage and transport channels for lithium ions. Meanwhile, the exchange current density i_0 exchange current density (i_0) is one of key parameters that influences the rate of a charge transfer controlled electrochemical reaction and can be calculated according to equation $i_0 = RT/nFR_{ct}$,[53] where R is the gas constant, T is the absolute temperature, n is the number of transferred electrons and F is the Faraday constant. As seen from Table 2, the HDPC electrode shows the highest value of exchange current density i_0, demonstrating that the electrochemical activity of HDPC is much higher than that of other two samples.

These results reveal that the well-formed porous structure combined with N- and S- doping effects of HDPC can afford lithium ions less resistance in short channels, leading to a higher rate capability.

Table 2 Kinetic parameters derived from the Nyquist plots for the samples

	R_e (Ω)	R_f (Ω)	R_{ct} (Ω)	i_0 (mA cm^{-2})
NH-C	4.58	12.31	55.11	0.466
AH-C	4.26	11.16	30.58	0.840
HDPC	4.31	9.35	18.23	1.409

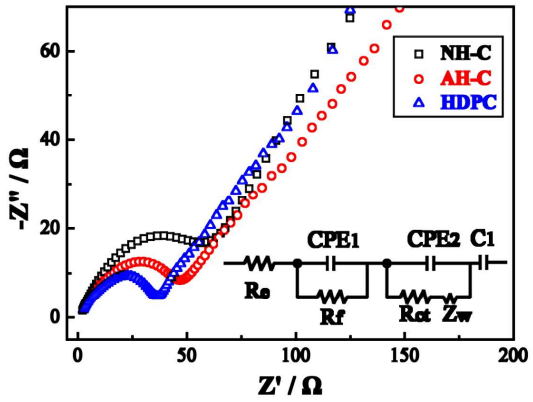

Fig. 7 Typical Nyquist plots recorded for the NH-C, AH-C and HDPC.

Acid pretreatment plays an important role in HDPC preparation. According to the paper, besides a large amount of protein, human hair contains trace amounts of metallic elements (such as Fe, Mn, As, Cr, and Ca),[30] which are closely associated with human health. These elements may hinder the channels of Li-ion diffusion. According to EDS results and total XPS spectrum (Table S1 and Fig. S3 ESI†), the elimination of these elements can be observed, which could produce more active sites for Li storage, thus enhancing the capacity of the carbon-based material. Moreover, with the removal of metallic elements, the hair became softer, making the permeation of porogens easier, which is essential for achieving high-quality pores. During the KOH treatment and high-temperature pyrolysis which followed, the KOH not only acted as a porogenic agent, but also caused swelling. This leads to a higher specific surface area than that of the sample without treatment of acid. Meanwhile, our results indicate that the acid pretreatment is vital, as the surface area of the target product (HDPC) reaches 1250 m^2 g^{-1}(pore volume 0.66 cm^3 g^{-1}) as compared to 1070 m^2 g^{-1} (pore volume 0.53 cm^3 g^{-1}) for the sample without acid pretreatment (AH-C) (seen in Table 1). Moreover, the removal of metallic elements could slightly increase the contents of N and S, which additional contributes to exceptional electrochemical performance.[32-33, 36]

The ultrahigh reversible capacity and excellent rate capability of HDPC can be reasonable explained as follows. First of all, 3D porous nanostructures combined with high specific surface areas can not only shorten the transport length for lithium ions but also offer large electrode/electrolyte interface for the charge-transfer reaction, as shown in Fig. 8. The hierarchical porous architecture composed of both micropores and mesopores plays important

roles in Li-ion storage. In this case, large amount of micropores are regarded as charge accommodation which is essential for high Li storage. Small amount of mesopores can provide expedite channels for organic electrolyte transportation and lithium ion diffusion, thereby increasing the number of active sites of the insertion and extraction of the Li-ions.[6,8,41] Moreover, the interconnected pores provide a continuous pathway for electron transport. Secondly, metallic elements in the human hair, which may occupy active sites and affect the lithium ion intercalation and deintercalation, are eliminated by the pretreatment of hydrochloric acid. This process can remove the metallic elements, and facilitate the activation by KOH, leading to the formation of high specific surface area and thus providing a high electrode/electrolyte contact interface. Last but not least, N and S incorporated in the matrix of carbon can enhance the electrochemical reactivity and electronic conductivity, which is favorable for the Li-ion storage capacity.

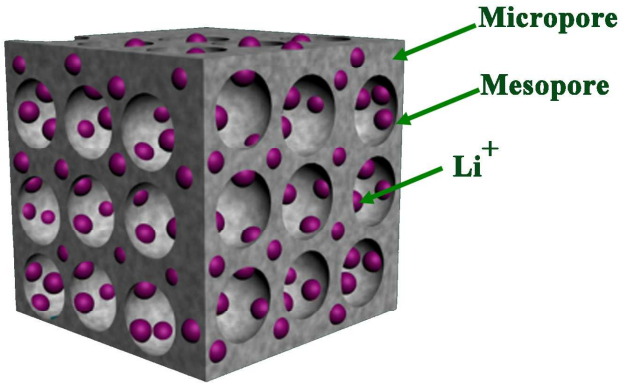

Fig. 8 Schematic representation of the micro/mesoporous structure and Li-ion storage in the HDPC.

Conclusions

In this paper, heteroatom doped porous carbon (HDPC) has been successfully prepared from human hair by a facile, economical and effective method. Acid pretreatment is introduced before KOH activation, contributes to the decrease of metallic elements and further promotes the activated process. In addition, without any extraneous doping, the contents of N and S are as high as 4.24% and 2.23%, respectively. The unique micro- and mesoporous structure, large surface area, and appropriate heteroatom introduction facilitate the transportation of the electrolyte and enhance the lithium ion insertion–extraction kinetics. The as-obtained HDPC exhibits superior performance as an anode material for LIBs with high reversible capacity (1331 mAh g^{-1} at 0.1 A g^{-1}) and excellent rate capability (205 mAh g^{-1} at 10 A g^{-1}). It is indicated that exploitation of low-cost precursors and universal nature resource is good way for the preparation of high-performance anode materials for LIBs. This approach also makes the carbon material possible for mass production. Furthermore, HDPC can also be applied in water purification, CO_2 capture and fuel cells.

Acknowledgements

We greatly appreciate the Natural Science Foundation of China (21275104, 21177090 and 21175094) for supporting this work.

Notes and references

[a] *College of Chemical Engineering, Sichuan University, No.24 South Section 1, Yihuan Road, Chengdu 610065, PR China. Fax: +86-28-85412907; Tel: +86-28-85416218*
[b] *Institute of New Energy and Low-Carbon Technology, Sichuan University, No.24 South Section 1, Yihuan Road, Chengdu 610065, PR China. Fax:+ 86-28-6213-8325; Tel: +86-28-6213-8375*
[c] *College of Chemistry, Sichuan University, 29 Wangjiang Road, Chengdu 610064, PR China. Fax: +86-28-85416029; Tel: +86-28-85416029*
**Corresponding author: Dan Xiao; E-mail: xiaodan@scu.edu.cn;*

References

1 J. M. Tarascon, M. Armand, *Nature*, 2001, **414**, 359.
2 J. R. Dahn,. T. Zheng, Y. Liu and J. S Xue, *Science*, 1995, **270,** 590.
3 M. Winter, O. J. Besenhard, M. E. Spahr and P. Novak, *Adv. Mater.,* 1998, **10,** 725.
4 N. A. Kaskhedikar, J. Maier, *Adv. Mater.,* 2009, **21,** 2664.
5 F. D. Han, Y. J. Bai, R. Liu, B. Yao, Y. X. Qi, N. Lun, et al., *Adv. Energy Mater.,* 2011, **1,** 798.
6 L. Qie, W. M. Chen, Z. H. Wang, Q. G. Shao, X. Li, L. X. Yuan, X. L. Hu, W. X. Zhang and Y. H. Huang, *Adv. Mater.,* 2012, **24,** 2047.
7 Y. S. Hu, P. Adelhelm, B. M. Smarsly, S. Hore, M. Antonietti and J. Maier, *Adv. Funct. Mater.,* 2007, **17,** 1873.
8 L. Ji, Z. Lin, M. Alcoutlabi, X. Zhang, *Energy Environ. Sci.,* 2011, **4,** 2682.
9 M. S. Kim, B. Z. Fang, D. S. Yang, T. S. Bae, J. S. Yu, *Langmuir*, 2013, **29**, 6754.
10 C. J. Meyers, S. D. Shah, S. C. Patel, R. M. Sneeringer, C. A. Bessel, N. R. Dollahon, R. A. Leising, E. S. Takeuchi, *J. Phys. Chem. B* 2001, **105,** 2143.
11 K. T. Lee, J. C. Lytle, N. S. Ergang, S. M. Oh, A. Stein, *Adv. Funct. Mater.,* 2005, **15,** 547.
12 F. Q. Zhang, Y. Meng, D. Gu, Y. Yan, C. Z. Yu, B. Tu, D. Y. Zhao, *J. Am. Chem. Soc.,* 2005, **127,** 13508.
13 B. Hu, K. Wang, L. Wu, S. H. Yu, M. Antonietti and M. M. Titirici, *Adv. Mater.,* 2010, **22,** 813.
14 B. Hu, S. H. Yu, K. Wang, L. Liu and X. W. Xu, *Dalton Trans.,* 2008, **40,** 5414.
15 E. Peled, V. Eshkenazi, Y. Rosenberg, *J. Power Sources,* 1998, **76,** 153.
16 S. H. Guo, J. H. Peng, W. Li, K. B. Yang, L. B. Zhang, S. M. Zhang, H. Y. Xia, *Appl. Surf. Sci.,* 2009, **255,** 8443.
17 W. Z. Shen, Z. F. Qin, H. G. Wang, Y. H. Liu, Q. J. Guo, Y. L. Zhang , *Colloids Surf. A,* 2008, **316,** 313.
18 Y. J. Hwang, S. K. Jeong, K. S. Nahm, J. S. Shin, A. M. Stephan, *J. Phys. Chem. Solids,* 2007, **68,** 182.
19 A. M. Stephan, T. P. Kumar, R. Ramesh, S. Thomas, A. K. Jeong, K. S. Nahm, *Mater. Sci. Eng. A,* 2006, **430,** 132.
20 G. T. Fey and C. Chen, *J. Power Sources,* 2001, **47,** 97.
21 F. Zhang, K. X. Wang, G. D. Li and J. S. Chen, *Electrochem. Commun.,* 2009, **11,** 130.
22 X. L. Wu, L. L. Chen, S. Xin, Y. G. Guo, Q. S. Kong, Y. Z. Xia, *ChemSusChem,* 2010, **3,** 703.
23 J. C.Arrebola, A. Caballero, et al., *J. Electrochem.Soc.,* 2010, **157,** A791.
24 A. Caballero, et al., *ChemSusChem,* 2011, **4,** 658.
25 Y. J Hwang, S. K. Jeong, K. S. Nahm, J. S. Shin and A. M. Stephan, *J. Phys. Chem. Solids,* 2007, **68,** 182.
26 L. Chen, Y. Z. Zhang, C. H. Lin and D. Xiao, *J. Mater. Chem. A*, 2014, **2,** 9684.

27 F. Baltenneck, B. A. Bernard, J. C. Garson, P. Engstrom, C. Riekel, F. Leroy, A. Franbourg and J. Doucet, *Cell. Mol.Biol.,* 2000, **46,** 1017.
28 J. W. S. Hearle, *J. Biol. Macromol.,* 2000, **27,** 123.
29 L. D. Lee and H. P. Baden, *Int. J. Dermatol.,* 1975, **14,** 161.
30 W. J. Qian, F. X. Sun, Y. H. Xu, L. H. Qiu and F. Yan, *Energy Environ. Sci.,* 2014, **7,** 379.
31 K. N. Chaudhari, M. Y. Song and J. S. Yu, *Small,* 2014, **10,** 2625.
32 Z. Li, Z. W. Xu, X. H. Tan, H. L. Wang, C. M. B. Holt, T. Stephenson, B. C. Olsen and M. Mitlin, *Energy Environ. Sci.,* 2013, **6,** 871.
33 D. S. Geng, H. Liu, Y. Chen, R. Y. Li, X. L. Sun, S. Ye and S. Knights, *J. Power Sources,* 2010, **196,** 1795.
34 M. Endo, C. Kim, T. Karaki, Y. Nishimura, M. J. Matthews, S. D. M. Brown and M. S. Dresselhaus, *Carbon,* 1999, **37,** 561.
35 Y. P. Wu, S. B. Fang and Y. Y. Jiang, *J. Mater. Chem.,* 1998, **8,** 2223.
36 Y. P. Wu, S. B. Fang and Y. Y. Jiang, and R. Holze, *J. Power Sources,* 2002, **108,** 245-249.
37 J. Wang, S. Kaskel, *J. Mater. Chem.,* 2012, **22,** 23710.
38 D. Y. Pan, S. Wang, B. Zhao, M. H. Wu, H. J. Zhang, Y. Wang and Z. Jiao, *Chem. Mater.,* 2009, **21,** 3136.
39 A. Ferrari and C. J. Robertson, *Phys. Rev. B: Condens. Matter Mater. Phys.,* 2000, **61,** 14095.
40 F. Tuinstra and J. L. Koenig, *J. Chem. Phys.,* 1970, **53,** 1126.
41 D. W. Wang, F. Li, M. Liu, G. Q. Lu and H. M. Cheng, *Angew. Chem., Int. Ed.,* 2008, **47,** 373.
42 W. H. Shin, H. M. Jeong, B. G. Kim, J. K. Kang, J. W. Choi, *Nano Lett.,* 2012, **12,** 2283.
43 C. C. Ma, X. H. Shao and D. P. Cao, *J. Mater. Chem.,* 2012, **22,** 8911.
44 L. Hao, X. Li and L. Zhi, *Adv. Mater.,* 2013, **25,** 3899.
45 J. Liang , Y. Jiao , M. Jaroniec , S. Z. Qiao , *Angew. Chem., Int. Ed.,* 2012, **51,** 11496.
46 Z. Yang, Z. Yao, G. Li, G. Fang, H. Nie, Z. Liu, et al., *ACS Nano,*. 2012, **6,** 205.
47 G. Ji, Y. Ma and J. Y. Lee, *J. Mater. Chem.,* 2011, **11,** 9819.
48 C. H. Huang, Q. Zhang, T. C. Chou, C. M. Chen, D. S. Su and R. A. Doong, *ChemSusChem,* 2012, **5,** 563.
49 J. Yi, X. Li, S. Hu, W. Li, L. Zhou, M. Xu, J. Lei and L. Hao, *J. Power Sources,* 2011, **196,** 6670.
50 D. Lu, W. Li, X. Zuo, Z. Yuan and Q. Huang, *J. Phys. Chem. C,* 2007, **111,** 12067.
51 Z. S. Wu, W. B. Ren, L. Xu, F. Li and H. M. Cheng, *ACS Nano,* 2011, **5,** 5463.
52 X. L. Ma, G. G. Ning, Y. Z. Sun, Y. J. Pu and J. S. Gao, *Carbon,* 2014, **79,** 310.
53 G. D. Li, L. Q. Xu, Q. Hao, M. Wang, Y. T. Qian, *RSC Advances,* 2012, **2,** 284.